Fuel 330 (2022) 125428

Contents lists available at ScienceDirect

Fuel

journal homepage: www.elsevier.com/locate/fuel

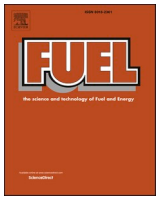

A comprehensive comparative study on methylene blue removal from aqueous solution using biochars produced from rapeseed, whitewood, and seaweed via different thermal conversion technologies

Fatih Güleç [a], Orla Williams [a], Emily T. Kostas [b], Abby Samson [c], Lee A. Stevens [d], Edward Lester [a]

[a] Advanced Materials Research Group, Faculty of Engineering, University of Nottingham, Nottingham NG7 2RD, UK
[b] Advanced Centre of Biochemical Engineering, Bernard Katz Building, University College London, Gower Street, London WC1H 6BT, UK
[c] Department of Mechanical Engineering, University of Sheffield, Sheffield S3 7RD, UK
[d] Low Carbon Energy and Resources Technologies Group, Faculty of Engineering, University of Nottingham, Nottingham NG7 2TU, UK

ARTICLE INFO

Keywords:
Biochar
Hydrothermal conversion
Pyrolysis
Torrefaction
Wastewater treatment Methylene blue
Adsorption

ABSTRACT

This paper presents, for the first time, a comprehensive comparative analysis of the potential of using biochars from three distinctly different UK-sourced biomass feedstocks, produced via three different thermal processing techniques, to adsorb methylene blue dye. Biochars were made from rapeseed, whitewood, and seaweed (*Laminaria Digitata*), produced via hydrothermal conversion, pyrolysis, and torrefaction. Adsorption kinetic models were developed for each biochar at different temperatures, pH and initial dye concentrations. Relatively high levels of methylene blue adsorption capacity were achieved by seaweed-based biochars (~150 mg/g), with reasonable levels for rapeseed-based biochars (~60 mg/g), whilst adsorption levels were found to be relatively low for whitewood-based biochars (<30 mg/g). A Pseudo-second-order kinetic model provided the best fit with experimental results. The Langmuir adsorption isotherm showed a better fit for seaweed biochars, while the Freundlich adsorption isotherm was a better fit for the rapeseed-based biochars. The Langmuir adsorption isotherms showed relatively high maximum adsorption capacity (Q^o) for seaweed-based biochars; ~175 mg/g for seaweed-Torrefaction and ~ 117 mg/g for seaweed-Pyrolysis. Negative Gibbs free energy (ΔG°) values were observed for the seaweed-Torrefaction < seaweed-Pyrolysis < 0, which indicates that the methylene blue removal could be a thermodynamically favourable process due to the spontaneous nature of the adsorption. Our investigation has shown that the removal of methylene blue from wastewater could be a potential application for seaweed-based biochars as part of a holistic whole life cycle valorisation pathway. However, it is not suitable for all types of biomasses which emphasises the need for tailoring unique valorisation pathways for different types of biomasses.

1. Introduction

Biochars have great potential as a low-cost adsorbent because of their availability, and inherent pore structure that can be modified to create relatively high surface area material [1]. Biomass feedstocks are relatively inexpensive and sustainable materials and are composed of three major components – hemicellulose, cellulose, and lignin [2,3]. Biochars are porous carbon-rich materials, produced via the thermochemical conversion of biomass below 700 °C in a low oxygen atmosphere [4]. Biochar characteristically has relatively high energy densities, calorific values, large surface areas, and abundant surface functional groups, which make them effective, low-cost, and environment-friendly carbonaceous materials [5,6]. Pyrolysis, torrefaction, and hydrothermal conversion are the most common thermal conversion technologies to convert biomass feedstocks to "biochar", "bio-oil", and "biogas" and the yield of these primary products depends on the process conditions. Whilst numerous studies exist on individual biomasses and/or thermal techniques [4,7–9], to date no study has comprehensively compared the adsorption potential of biochars from different feedstocks prepared using all three thermal processing techniques.

Slow pyrolysis produces maximum biochar yields, with optimal process temperatures ca. 400 °C, a slow heating rate (2–7 °C/min), and long residence times (hours to days) under an oxygen-free environment [10]. Torrefaction also converts biomass feedstocks into medium-grade solid products (biochars) with a process temperature of 200–300 °C

E-mail addresses: Fatih.Gulec1@nottingham.ac.uk, Gulec.Fatih@outlook.com (F. Güleç).

https://doi.org/10.1016/j.fuel.2022.125428
Received 30 May 2022; Received in revised form 16 July 2022; Accepted 25 July 2022
Available online 10 August 2022

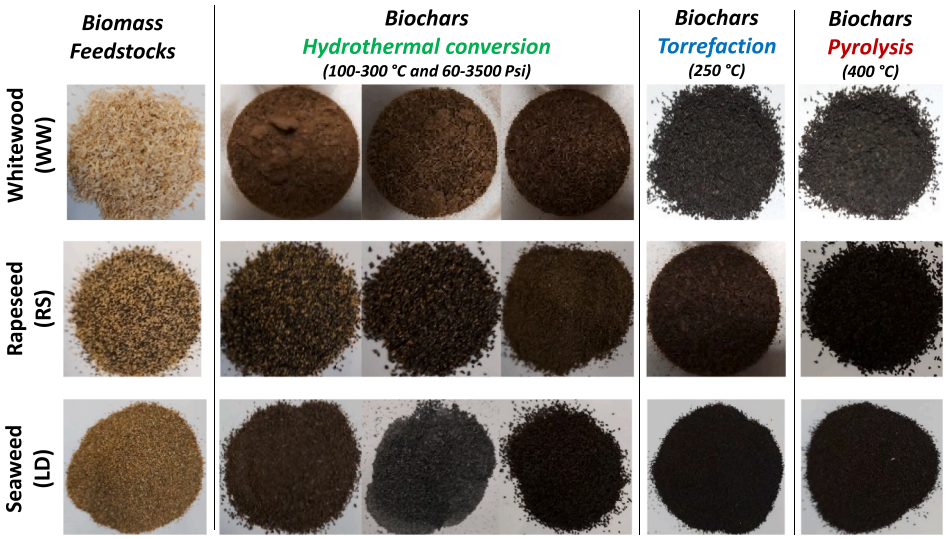

Fig. 1. Biomass feedstocks (LD, RS and WW) and biochars produced from these biomass feedstocks through hydrothermal conversion, pyrolysis, and torrefaction.

under low-oxygen or inert atmospheres by removing the moisture and low energy volatiles from biomass [10]. Hydrothermal carbonisation (HTC) is an alternative method of producing biochars with a low-temperature hydrothermal conversion under sub-critical conditions (180–250 °C, 15–40 bar) [11,12]. Pyrolysis and torrefaction processes are usually conducted with low moisture content biomass, whereas hydrothermal conversion is used for the high moisture content biomass [13]. Hydrothermal conversion can be done in three forms: hydrothermal carbonisation (180 °C, 15–40 bar), liquefaction (250–370 °C, 25–240 bar) and gasification (350–700 °C, <300 bar) [14]. Hydrothermal conversion facilitates the physio-chemical transformation of biomass in hot-compressed water to produce biochars, bio-oil, and biogas, as well as value-added chemicals (ethanol, acetone, acetic acid etc.) [15]. Most studies focus on comparisons of pyrolysis and torrefaction to hydrothermal carbonisation and/or single biomass feedstock types or groups [16,17]. Currently, only limited studies compare the three-carbonisation techniques for biochars production for dye removal [18].

Biomass feedstock type, conversion process, and process conditions such as temperature, pressure, residence time, and heat transfer rate have a major effect on the physicochemical properties of biochars [19] surface area, pore structure, carbon content, and surface functional groups [20,21]. As these physicochemical properties play a crucial role in determining the performance of these biomass/biochars, process conditions are of critical importance. The surface area, carbon content and pore structure can be enhanced by increasing the pyrolysis temperature [22] but it also results in a reduced char yield [10]. Furthermore, a slow heating rate eliminates secondary pyrolysis reactions and cracking, which maximises char yield [23], and favours the formation of a stable matrix within the biochar [24]. Biobased carbon materials (i.e. biochars, activated carbon) have a wide range of applications such as soil supplements [25,26], an adsorbent to remove the pollutants from soil and wastewater, and renewable energy production to produce electricity and heat via combustion [27–30], hydrogen storage [31]. Identification of the most suitable application technology of biochar produced with a specific biomass processing technology is crucial to the use of full valorisation of the biomass and potentially decreases the cost of the biomass processing technology [32,33]. As biomass processing technologies need to take a broad life cycle assessment approach [34] to ensure economic sustainability by maximising the potential of feedstock valorisation.

Dye contamination in wastewater streams of textile industries is a crucial environmental concern [35,36]. Extensive research has been carried out on the removal of methylene blue (MB) dye by various sorbents i.e. activated carbon [36–39], biochar [40,41], biomass [42–47], composites materials [48–50]. Among these sorbents, biochars/biomass provides promising results in the application of dye removal from wastewater [50,51] in a holistic approach due to their low cost, availability, and effectiveness. As compared to traditional ion exchange resins and commercial activated carbons, bio-sorbents often show higher selectivity in dye removal [52]. Extensive research has therefore been carried out for the removal of MB by various biomass and biochars including silk powder [53], orange peel [54], pine tree leaves [55], green macroalga Caulerpa lentillifera [56], Sargassum muticum [47] and many others [44,45,50,53,54,57]. Jawad et al. [40] investigated the removal of MB with acid-functionalised bio-sorbent produced from a waste coconut shell by chemical treatment. Chemically treated coconut shell demonstrated an MB adsorption capacity of 50.6 mg/g at 303 K. The adsorption mechanisms of MB over the bio-sorbent were associated with the interactions on the surface such as H-bonding, electrostatic attractions, and π-π interaction [40]. Shau et al. [57] also produced biochar from lychee seed by chemical activation and the biochars provided an MB adsorption capacity of 124.5 mg/g based on the Langmuir isotherm model. Furthermore, bio-adsorbents derived from suitable algal biomass showed an affective removal of MB [52], i.e. the adsorption performance of green macroalga Caulerpa *lentillifera* (417 mg/g) [56], Sargassum *muticum* (279 mg/g) [47], and Fomes *fomentarius* (232 mg/g) [58]. Removal of MB with bio-sorbents is a promising method, which is particularly suitable for the treatment of low concentrations of MB [52]. It also could be one of the holistic approaches to minimise the cost of biomass processing technologies using solid residues (or biochars) for dye removal [32,33].

This paper presents a comparative study on how the optimal holistic biomass processing pathways and process interdependencies influence the MB dye adsorption properties of biochars made from three distinctly different biomass feedstocks. The suitability of three distinctly different UK sourced biomass feedstocks (Whitewood, Rapeseed, and Seaweed (Laminaria *Digitata*)) were investigated for biochar formation in three commonly used thermal conversion technologies; torrefaction, pyrolysis, and hydrothermal conversion (subcritical conditions; hydrolysis, carbonisation, and liquefaction) under a wide range of processing conditions. The study looks at the effects of pH, temperature, and concentration. Furthermore, the biochar adsorption kinetics, adsorption equilibrium models, and adsorption thermodynamics were also investigated to identify the kinetics and equilibrium models of the biochars.

2. Material and methods

2.1. Biomass feedstocks and thermal conversions

Three different biomass feedstocks were used in this study (provided in Fig. 1). Rapeseed residues (RS) as a source of agricultural waste were supplied by the School of Biosciences at the University of Nottingham. The rape seed (Brassica napus L., variety DK Exalte) was provided by a local farm following the 2017 summer harvest and stored at 20 °C and rH 50 % until use [59,60]. The RS was obtained by the modified method presented in Ref. [59,60]. Whitewood (WW, made from sawdust residues from Northern Ireland (UK), supplied by Wolseley). The brown seaweed (Laminaria digitata, LD) was collected at low spring tides in May 2015 near Downderry in Cornwall (UK) (GPS coordinates: 50.3623° N. 4.3687° W) and prepared by following the methods outlined in Ref [61]. These feedstocks were selected as they are all domestically produced in the UK and from three distinct types of biomasses [3,61,62].

The hydrothermal conversion of RS, LD and WW was investigated at low to medium temperatures (100 °C for hydrolysis, 200 °C for carbonisation, and 300 °C for liquefaction) under a wide range of pressures (60 – 3500 psi) using a semi-continuous hydrothermal rig, illustrated previously [15], to establish the optimal conditions for biochar production. The biochar formation from RS, LD, and WW via pyrolysis was investigated in a micro-activity fixed bed unit, illustrated previously [63–66], at 300, 400 and 550 °C for 60 min under a N_2 flow of 12 ml/min. Torrefaction of biomass feedstocks (LD, RS and WW) was also investigated in a horizontal tube furnace, illustrated previously [27,63], using the following procedure, the biomass resources were placed in the middle zone of a quartz reactor, heated from ambient temperature to the torrefaction temperatures of 220, 250 and 280 °C with a heating rate of 10 °C/min under an N_2 flow rate of 1.0 L/min and the temperature was maintained at this level for 60 min. Further details about the hydrothermal process, pyrolysis and torrefaction and operating of these rigs were presented previously [32,33]. The abbreviations “HC”, “PC” and “TC” are used in the following sections to represent the biochars (Fig. 1) produced by hydrothermal conversion, pyrolysis, and torrefaction, respectively.

2.2. Characterisation of biochars

Proximate analysis of biomass feedstocks (RS, WW, LD) and prepared chars was performed in a TA-Q500 using the procedure described previously [15] as well methodologies for proximate and ultimate analysis [32,33]. Furthermore, the elemental compositions (carbon (C), hydrogen (H), nitrogen (N)) of biomass feedstocks were determined using LECO CHN 628 and oxygen (O) content was calculated by difference [67].

2.2.1. Textural properties

The textural properties (surface area and micropore volume) of prepared biochars were measured using a Micromeritics ASAP 2420 instrument (Micromeritics ltd) using CO_2 as the adsorbate. Before analysis, approximately 0.50 g of sample was degassed under a high vacuum (<0.013 mbar) at 120 °C for 15 h to remove adsorbed gases and moisture on the samples. CO_2 isotherms were acquired from 0.000005 to 0.034 relative pressure (0.00023–1.18115 bar) at 0 °C. The specific surface area of the samples was calculated using the BET model at 0.025 to 0.030 relative pressure (0.83–1.07 bar) and the micropore volume by the Dubinin-Radushkevich model using Microactive Software V5.0 [68].

2.2.2. FTIR analysis

The infrared spectrums of biomass feedstocks and chars were scanned using a Bruker IFS66 (FTIR) with KBr beam splitter, Globar light source, deuterated triglycine sulfate (DTGS) room temperature detector and Specac “Goldengate Bridge” diamond attenuated total reflection (ATR) attachment. The instrument was air purged by a Parker Balston 75–52 FTIR purge gas generator. The dried samples were scanned with a resolution of 8 cm^{-1} within the infrared region of 400–4000 cm^{-1}. For the RS samples, background and sample were both collected for 119 scans (1 min), for the WW and LD samples 238 scans (2 min) were used.

2.3. Wastewater treatment application of biochars

Adsorption experiments were carried out using methylene blue dye (MB) from Sigma Aldrich. Initially, the effects of particle size on dye adsorption for the pre-processed biomass were investigated to identify the mass limitations in the process. The effects of pH, temperature and initial MB concentration were investigated for the pre-processed biomass feedstocks, biochars (produced in hydrothermal conversion at 200 °C under 3500 psi, produced in pyrolysis at 400 °C, and produced in torrefaction at 250 °C) of RS, WW and LD.

2.3.1. Effects of pH

To investigate the effects of pH, 10 mg of adsorbents (biomass feedstocks, biochars produced at 200 °C under 3500 psi in hydrothermal conversion, produced at 400 °C in pyrolysis, and produced at 250 °C in torrefaction, as representative of each thermal conversion technology) were placed in a glass cylindrical cell and mixed with 10 ml of 200 ppm initial MB concentration in a pH ranges of 2.0 – 10.0 in an incubator operating at 30 °C for 24 h. The pH of the experiment solutions was adjusted by 0.1 M HCl or 0.1 M NaOH solutions.

2.3.2. Effects of temperature and initial MB concentration

The adsorption experiments were repeated as per the pH experiments with approximately 30 mg of adsorbent and 30 ml of MB solution having an initial concentration of 200 ppm, 100 ppm and 50 ppm at a pH of 6.0. The adsorbents and MB solution were mixed in a glass baker at 160 rpm in an incubator operating at 20, 30, and 40 °C for 24 h. To demonstrate the adsorption curves and calculate the adsorption kinetics, approximately 140 μL (0.46 % of the total solution) of the samples were removed from the solution at specific time intervals using automatic pipettes.

2.3.3. Comparison of the adsorption capacities of biochars

The adsorption experiments were repeated with all the biochars produced at different temperatures in hydrothermal conversion, pyrolysis and torrefactions processes. Approximately 10 mg of biochar mixed with 10 ml of MB solution having an initial concentration of 100 ppm at 160 rpm and an initial pH of 6.0 in a glass cylindrical cell at 30 °C using an incubator for 24 h. After each run, the dye solution was filtrated using a syringe filter (20 μm of pore size) and the MB concentration was measured by Ultraviolet–Visible spectrophotometer (UV/Vis, Shimadzu UV mini-1240). One set of each experiment group was triplicated under identical conditions to determine the experimental error. The dye concentration at equilibrium was calculated from the calibration curve, which was obtained at the wavelength of maximum absorbance (664 nm). The dye removal efficiency (Eq-1) [55,69] and adsorption capacity (Eq-2) [55,69] were determined using the following equations.

$$Removal\ efficiency\ (wt.\%) = \frac{C_0 - C}{C_0} * 100 \quad (1)$$

$$q\ (mg/g) = \frac{(C_0 - C) * V_{sol}}{m_{ads}} \quad (2)$$

Where C_0 and C (mg/L) is the initial and residual MB concentration, V_{sol} (L) is the MB volume used in the adsorption, m_{ads} (g) is the mass of adsorbent (biomass feedstocks of char) used in the adsorption, q (mg/g) is the adsorption capacity of the adsorbent.

2.4. Adsorption kinetics, equilibrium models, and thermodynamics

2.4.1. Adsorption kinetics

Adsorption kinetics of biomass feedstocks and biochars were investigated using kinetic models. Pseudo-first order, pseudo-second-order, and intra-particle diffusion models were applied to the experimental data set produced at 30 °C for the initial MB concentration of 50, 100 and 200 ppm. As these models include the mass transfer steps during the adsorption process, they are a means of identifying the adsorption kinetics of dye removal processes. Additionally, these models specifically Pseudo-first order and pseudo-second-order are well-known adsorption kinetic models used in the predictions of adsorption rate in batch adsorbers [35,69,70]. The major limitations of Pseudo-first order and Pseudo-second order adsorption rate models were defined by Yener et al. [35,36] as in these models, the adsorption rate constant is relatively dependent on the adsorbate concentration and the amount of adsorbent charged to the adsorber. The non-linear and linearised equations of Pseudo-first order (Eq. (3) and Eq. (4)) and Pseudo-second order (Eq. (5) and Eq. (6)) kinetic models are presented below [69,70]. The intra-particle diffusion model can be presented in Eq. (7) [53,71].

- *Pseudo-first order*

$$\frac{dq}{dt} = k_{1,ad}(q_{eq} - q_t) \tag{3}$$

$$\log(q_{eq} - q_t) = \log(q_{eq}) - \frac{k_{1,ad}}{2.303}t \tag{4}$$

- *Pseudo-second order*

$$\frac{dq}{dt} = k_{2,ad}(q_{eq} - q_t)^2 \tag{5}$$

$$\frac{t}{q_t} = \frac{1}{k_{2,ad}q_{eq}^2} + \frac{1}{q_{eq}}t \tag{6}$$

- *Intra-particle diffusion*

$$q_t = k_{3,ad}\sqrt{t} + C \tag{7}$$

Where t (min) is the adsorption time. q_t (mg/g) is the adsorption capacity at a time. q_{eq} (mg/g) is the adsorption capacity of the adsorbent at the equilibrium point. $k_{1,ad}$ (1/min), $k_{2,ad}$ (g/mg.min), and $k_{3,ad}$ (mg/g.$min^{1/2}$) are the rate constant of pseudo-first-order, pseudo-second-order, and intra-particle diffusion models, respectively.

2.4.2. Adsorption equilibrium models

Type of adsorption equilibrium and maximum adsorption capacity of biomass feedstocks and chars were identified with Langmuir and Freundlich adsorption isotherms using the experimental data produced at 30 °C for the initial MB concentration of 50, 100, and 200 ppm. The amount of effluent at the solid–liquid interface increases non-linearly with the concentration at the equilibrium conditions. These models are the most frequently used models in the literature [42,46,53,55,57,71,72] to describe the non-linear equilibrium between q_{eq} and C_{eq} at a constant temperature. The non-linear and linearised equations of Langmuir (Eq-8 and Eq-9) and Freundlich (Eq-10 and Eq-11) adsorption models are presented below [69,70].

- *Langmuir Model*

$$q_{eq} = \frac{Q^0 b C_{eq}}{1 + b C_{eq}} \tag{8}$$

$$\frac{C_{eq}}{q_{eq}} = \frac{C_{eq}}{Q^0} + \frac{1}{Q^0 b} \tag{9}$$

- *Freundlich Model*

$$q_{eq} = K_F C_{eq}^{1/n} \tag{10}$$

$$ln(q_{eq}) = ln(K_F) + \frac{1}{n}ln(C_{eq}) \tag{11}$$

Where q_{eq} (mg/g) is the adsorption capacity of the adsorbent at the equilibrium. C_{eq} (mg/L) is the residual dye concentration at equilibrium. Q^0 is the maximum adsorption capacity. b is the adsorption bonding energy. K_F ((mg/g.(mg/L)^n) is the Freundlich adsorption constant. n is the Freundlich adsorption constant.

2.4.3. Adsorption thermodynamics

Thermodynamic parameters of an adsorption process shows whether the process is favourable [55]. The thermodynamic parameters of Gibbs free energy change ΔG°, standard enthalpy ΔH°, and standard entropy ΔS° of the kinetic data were therefore analysed to gain a greater insight into the effect of temperature on the adsorption. The thermodynamic parameters ΔG°, ΔH°, and ΔS° were determined using the following equations [55]:

$$K_d = q_{eq}/C_{eq} \tag{12}$$

$$\ln K_d = \frac{\Delta S^o}{R} - \frac{\Delta H^o}{RT} \tag{13}$$

$$\Delta G^o = \Delta H^o - T^*\Delta S^o \tag{14}$$

Where T is the adsorption temperature (K), R is the ideal gas constant (8.314 J/mol K), and K_d is the distribution coefficient.

3. Results and discussions

3.1. Characterisation of feedstocks

The ultimate analysis, proximate analysis, and densities of biomass feedstocks are presented in Table S1. The ultimate analysis shows a wide range of carbon and oxygen compositions for these biomass feedstocks. WW and RS have the highest volatile matter (~79 wt%) and lowest fixed carbon (~11–13 wt%) ratios while LD provides lower volatile matter (~55 wt%) and higher fixed carbon of ~ 29 wt%. Furthermore, the LD has a relatively high ash content (~7.4 wt%) compared to the other samples. LD also had higher tap (0.83 g/cm^3) and true densities (1.62 g/cm^3) compared to RS and WW. Due to the differences in composition and physical properties of these biomass feedstocks, it was proposed that a wide range of char formation should be possible via hydrothermal conversion, pyrolysis, and torrefaction.

3.2. Thermal conversion of RS, WW, and LD to biochars

The production of biochars of RS, WW and LD produced via hydrothermal conversion, pyrolysis, and torrefaction is discussed in detail in previous works by the authors [32,33]. Fig. S1 in the supplemental information provides information on the biochar yields obtained from the three processes for the three-biomass feedstocks at a range of conditions. In summary, increasing the operating temperature of all the thermal conversion technologies decreased the biochar yield regardless of the technology, which is in agreement with previous findings [22,73]. All samples exhibited higher thermal decomposition under hydrothermal conversion compared to pyrolysis and torrefaction, and the increase in the operating temperature gradually decomposed the structure of the

Table 1
Biochars produced by different process conditions.

Process	Feedstocks	Conditions	Biochars and labels*
Torrefaction (TC)	L. Digitata (LD) Rapeseed (RS) Whitewood (WW)	T = 220, 250, 280 °C t = 60 min	•LD-TC-220 •LD-TC-250 •LD-TC-280 •RS-TC-220 •RS-TC-250 •RS-TC-280 •WW-TC-220 •WW-TC-250 •WW-TC-280
Pyrolysis (PC)	L.Digitata (LD) Rapeseed (RS) Whitewood (WW)	T = 250, 300, 400, 550 °C t = 60 min	•LD-PC-250 •LD-PC-300 •LD-PC-400 •RS-PC-300 •RS-PC-400 •RS-PC-550 •WW-PC-300 •WW-PC-400 •WW-PC-550
Hydrothermal (HC)	L.Digitata (LD) Rapeseed (RS) Whitewood (WW)	T = 100, 150, 180, 200, 235, 265, 300 °C t = 60 min	•LD-HC-100 •LD-HC-150 •LD-HC-180 •LD-HC-200 •LD-HC-300 •RS-HC-100 •RS-HC-200 •RS-HC-235 •RS-HC-265 •RS-HC-300 •WW-HC-200 •WW-HC-235 •WW-HC-265 •WW-HC-300

*Biochars were labelled as "BB-PP-TTT" in which "BB" represents the biomass feedstocks (LD for L. Digitata, RS for Rapeseed, and WW for Whitewood), "PP" represents the thermal conversion technologies ("TC" for Torrefaction, "PC" for Pyrolysis, and "HC" for hydrothermal conversion) and "TT" represents the process temperatures of the thermal conversion technologies.

biomass feedstocks. Hemicellulose structures are known to decompose at 220–315 °C, cellulose structures at 315–400° C and lignin structures decompose between 160 and 900 °C [74–80]. However, lower char yields were obtained via hydrothermal conversion compared to pyrolysis and torrefaction (Fig. S1). The extensive list of the biochars created by thermal conversion technologies is presented in Table 1. Among these biochars, biochars produced from all three biomass feedstocks via hydrothermal conversion at 200 °C (LD-HC-200, RS-HC-200, and WW-HC-200), pyrolysis at 400 °C (LD-PC-400, RS-PC-400, and WW-PC-400), and torrefaction at 250 °C (LD-TC-200, RS-TC-200, and WW-TC-200) were selected to investigate the effects of pH, temperature, initial MB concentration, kinetics and thermodynamics of MB adsorption. The rest of the biochars were tested in optimised conditions.

3.3. Characterisation of biochars

3.3.1. Surface area and pore structure

Surface area and micropore volumes for the biomass feedstocks and biochars produced via the three conversion technologies are presented in Fig. 2. The biochars produced from LD and RS via torrefaction (at 250 °C) provided a relatively high surface area (59 m^2/g for LD and 54 m^2/g for RS) compared to raw LD (3 m^2/g) and RS (4 m^2/g), as shown in Fig. 2a–b. Similarly, the surface area significantly increased via processing the LD and RS in pyrolysis at 300 °C (Fig. 2a–b). However, the biochars produced from WW via torrefaction (at 250 °C) and pyrolysis (at 300 °C) showed lower surface area (69–77 m^2/g) compared to raw WW (148 m^2/g). Regardless of biomass type (LD, RS, WW), the micropore volume was enhanced by torrefaction and pyrolysis processes. As for the hydrothermal conversion, both surface area and micropore

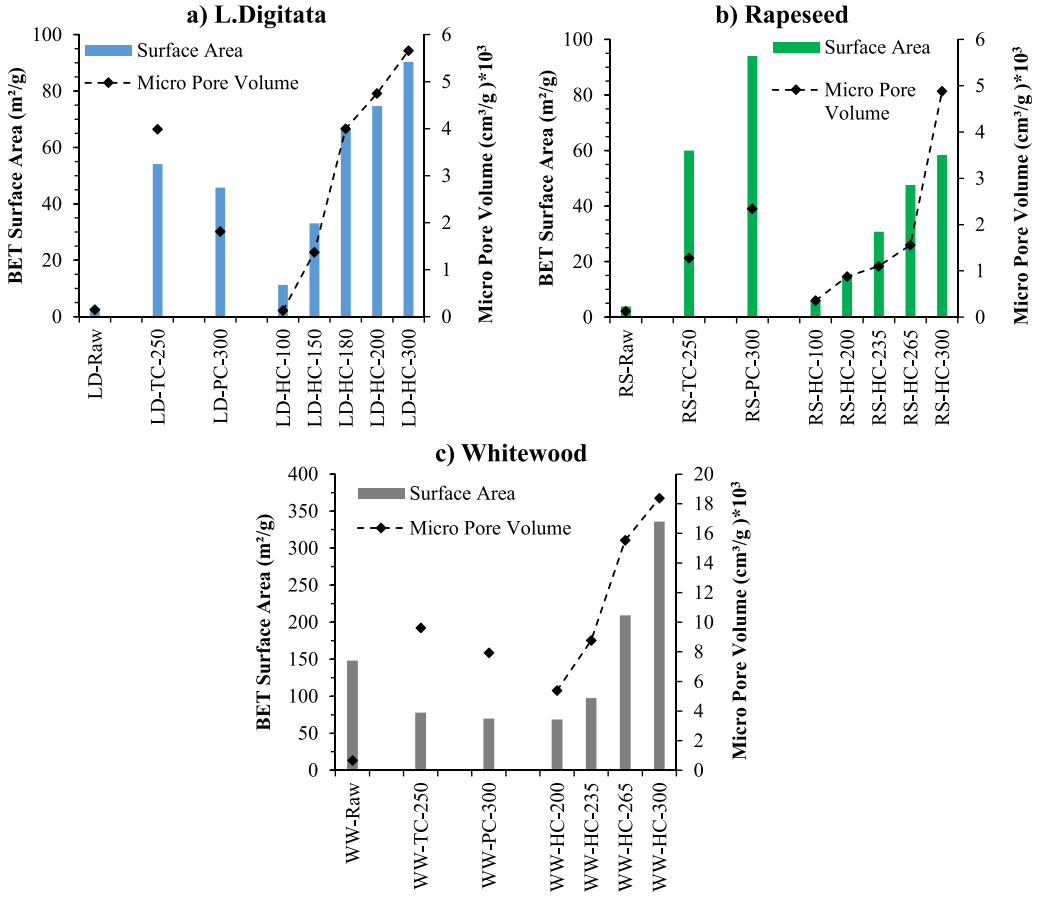

Fig. 2. Surface area and micropore volume (<1.118 nm) for the biomass feedstocks (LD, RS and WW) and biochars produced from these biomass feedstocks through hydrothermal conversion, pyrolysis, and torrefaction. The abbreviations "HC", "PC" and "TC" represent the biochars produced by hydrothermal conversion, pyrolysis, and torrefaction, respectively.

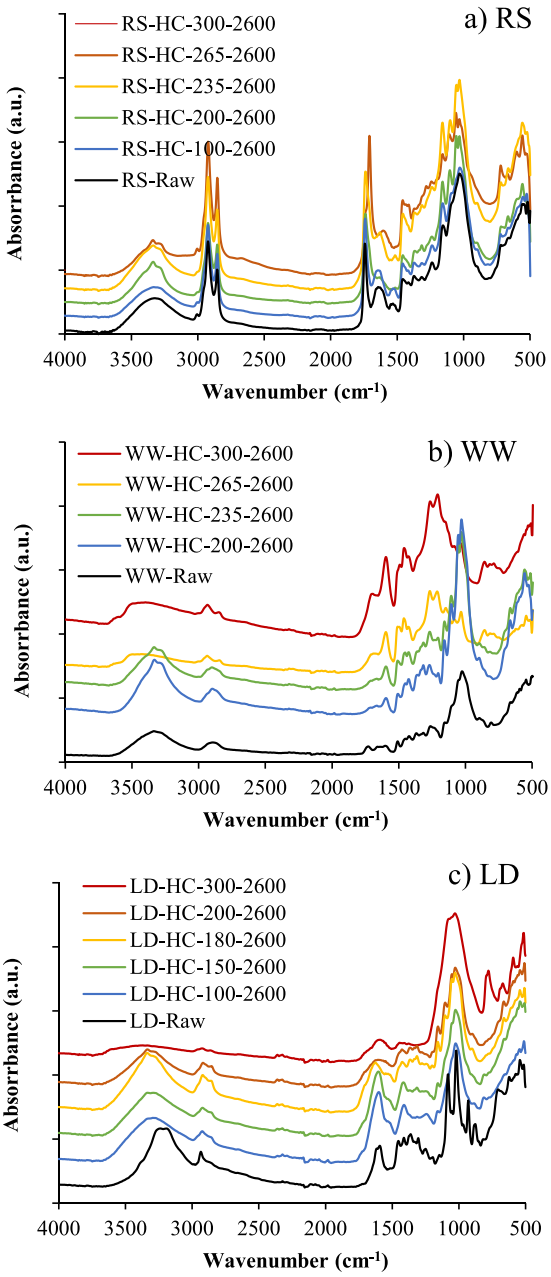

Fig. 3. FTIR analysis of biochars produced from a) RS, b) WW, and c) LD with hydrothermal conversion.

volume increased with increasing the process temperatures. The surface area of biochars increased from 11 to 90 m^2/g for LD, 5 to 58 m^2/g for RS, and 68 to 335 m^2/g for WW with increasing the hydrothermal conversion temperature from 100 to 300 °C. The surface area of biochar increases with increasing temperature, as the surface area increases from ~ 212 m^2/g and ~ 274 m^2/g for the RS and WW biochars produced via pyrolysis at 550 °C, which is similar to other studies [22]. Porosity, surface area, and pore matrix can be enhanced by selecting the right heating rate; higher heating rates provide higher porosity thanks to the rapid volatilisation while the slow heating rate results in a stable matrix formation [24].

3.3.2. *Fourier transforms infrared (FTIR) analysis*

FTIR analysis and peak assignments for the biomass feedstocks (LD, RS, and WW) are presented in detail in the Supplementary section (Fig. S2-S3 and Table S2) and compared against HC biochars in Fig. 3. The FTIR results of the other biochars produced by pyrolysis and torrefaction are presented in Supplementary Figures Fig. S2 and S3. Although the FTIR peaks identifies surface functional groups for each biochar, the intensity of these peaks shows the degradation, transformation, and potentially chemical reactions of main structures of biomass feedstocks (hemicellulose, cellulose, and lignin) [81]. Hydrothermal conversion has insignificant effect on the surface functional groups of biochars produced from RS up to 300 °C (Fig. 3a). However, the some of the functional groups have disappeared for the biochars, which are produced from LD at above 180 °C (Fig. 3c) and WW at above 235 °C (Fig. 3b). For example, the wide band (3100–3600 cm^{-1}) and the peak at 2935 cm^{-1}, which are associated with symmetric and asymmetric stretching vibrations of H_2O [82,83] or non-bounded –OH groups [84,85] and asymmetric C—H stretching of the aliphatic functional groups [84,86], are partially disappeared (Fig. 3b–c).

For the LD biochars, the intensity of the peak at ~ 1600 cm^{-1} increases with an increase in hydrothermal temperature up to 180 °C and the peaks between 800 and 1100 cm^{-1} are combined (Fig. 3c). The peak between 800 and 1100 cm^{-1} is shifted to a higher wavenumber ~ 1070–1275 cm^{-1} for the biochars produced at above 265 °C (Fig. 3b). This increase could be attributed to the increase in the lignin portion in the biochar, as the peak assigned to the C—O, C—O—C, and C-OH stretching vibration of the main source of cellulose, hemicellulose, and lignin [84,86–88]. The intensity of wide hydroxyl band (3100–3600 cm^{-1}) partially decreased with increasing pyrolysis temperature (Fig. S2) and torrefaction temperature (Fig. S3) for all biomass feedstocks, which could be attributed to a dehydration reaction. Additionally, the increase in the pyrolysis temperature decreases the intensity of peaks (Fig. S2), which could be attributed to the thermal decomposition of side chain and dehydration reaction of biomass feedstocks [81]. However, each feedstock (RS, WW, and LD) shows different levels of degradation by pyrolysis, which results different level of peak intensities. At the pyrolysis temperature of 550 °C, the peaks are completely gone for the RS and WW biochar (Fig. S2). The biochars produced with torrefaction provide similar peaks with the raw biomass feedstock and do not show a significant change through the torrefaction temperature (Fig. S3).

3.4. *Wastewater treatment – Methylene blue adsorption*

The first stage of the MB dye adsorption tests explored the influences of several parameters on the adsorption process for the biochars. The influence of initial MB concentrations, pH of the MB solution, and adsorption temperature was investigated using selected biochars (produced via hydrothermal conversion at 200 °C (LD-HC-200, RS-HC-200, and WW-HC-200), pyrolysis at 400 °C (LD-PC-400, RS-PC-400, and WW-PC-400), and torrefaction at 250 °C (LD-TC-200, RS-TC-200, and WW-TC-200). The aim was to find the relationship between biochar properties and optimal MB adsorption. Following this, kinetic and equilibrium models were developed for the selected biochars.

3.4.1. *Initial MB concentrations*

Initial concentrations of 50 ppm, 100 ppm and 200 ppm were tested to analyses the influence of MB concentration on uptake for the different biochars (Fig. 4). 50 ppm had the highest percentage removal for all biochars, and 200 ppm the lowest, although the difference varied by sample and processing technique. LD biochars produced by Torrefaction and Pyrolysis exhibit almost complete MB removal for all concentrations, but hydrochars produced by LD provide relatively lower MB removal, particularly as the MB concentration increased. RS showed large variances in uptake based on solution concentration, with 50 ppm resulting in uptakes between ~ 45 and 60 % (Fig. 4b), but only ~ 10–25 % for 200 ppm (Fig. 4b).

Despite the lower percentage uptakes for higher solution concentrations (Fig. 4), Fig. 5 illustrates that higher absorption capacity were observed in the higher MB concentration tests, which could be attributed to a driving force of mass transfer [42]. Similar observations were

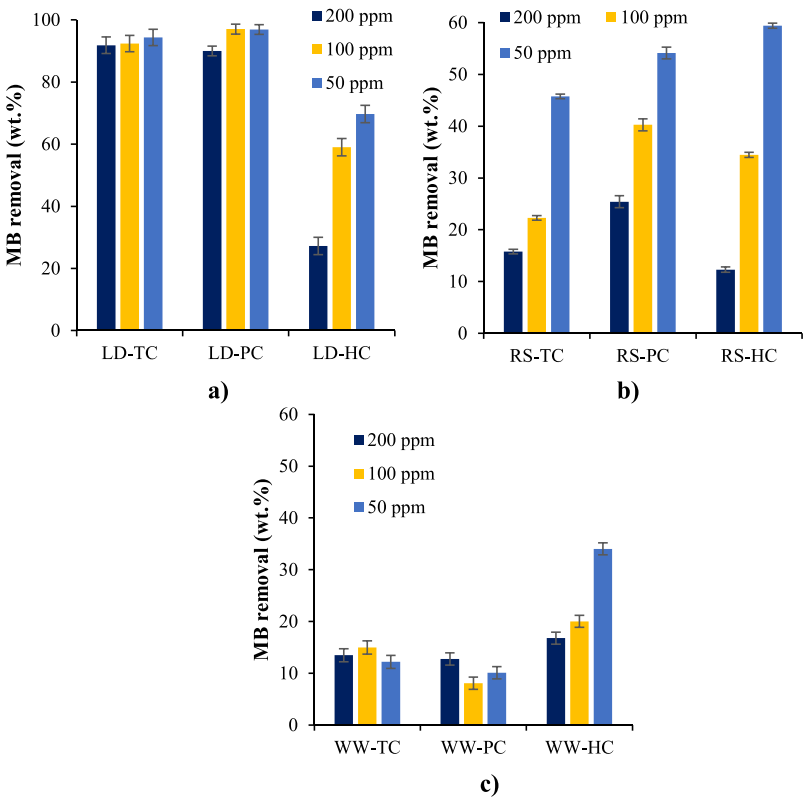

Fig. 4. Effects of initial MB concentrations (50–200 ppm) on removal efficiency of a) LD-based biochars, b) RS-based biochars, and c) WW-based biochars at 30 °C for 24 h.

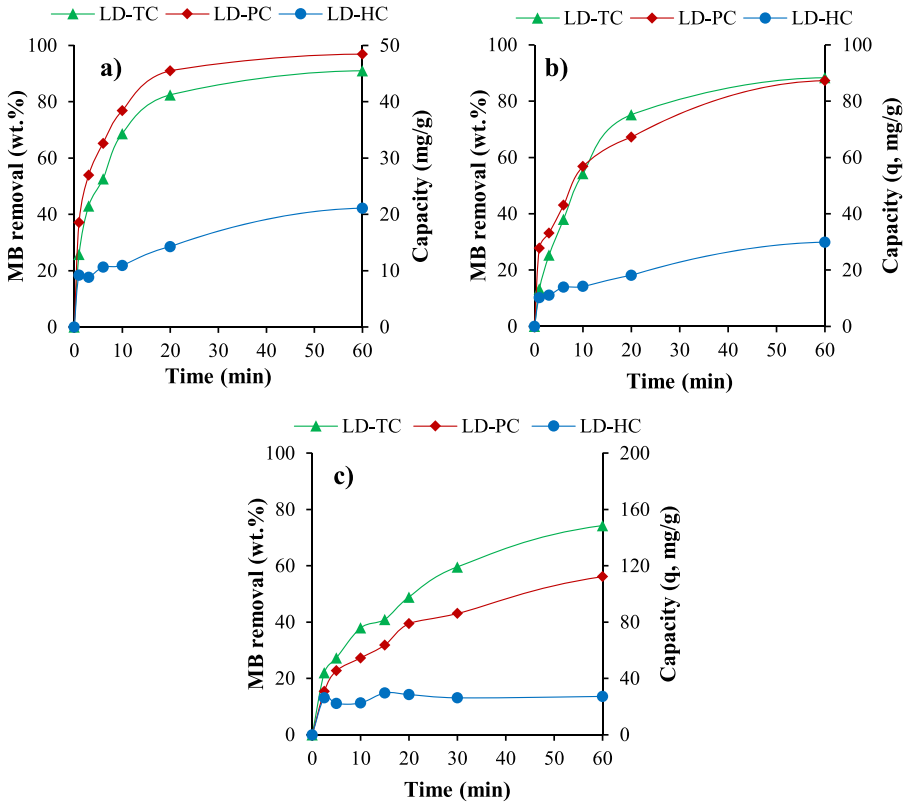

Fig. 5. MB removal and adsorption capacity isotherms of LD-based biochars at different initial MB concentrations a)50 ppm, b) 100 ppm, and c) 200 ppm at 30 °C for 60 min.

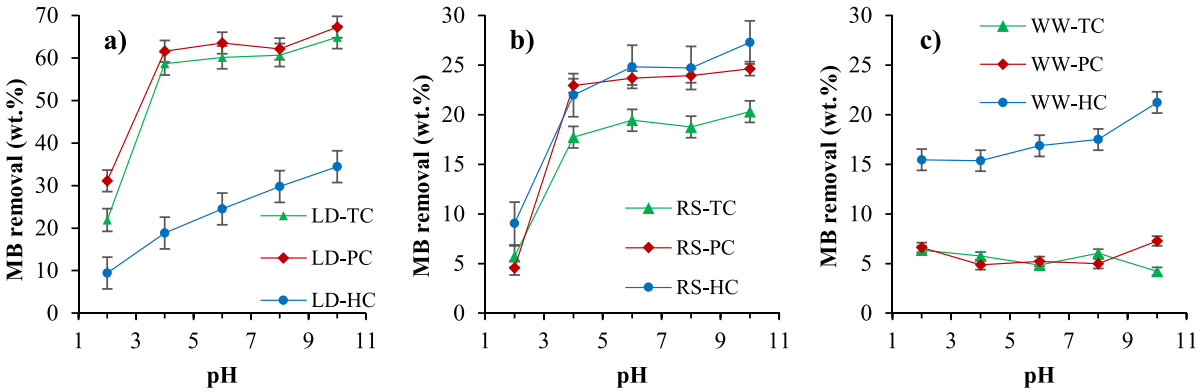

Fig. 6. Effects of initial pH of MB solution on dye removal and adsorption capacity of a) LD-based biochars, b) RS-based biochars, and c) WW-based biochars under 200 ppm of initial MB concentration for 24 h.

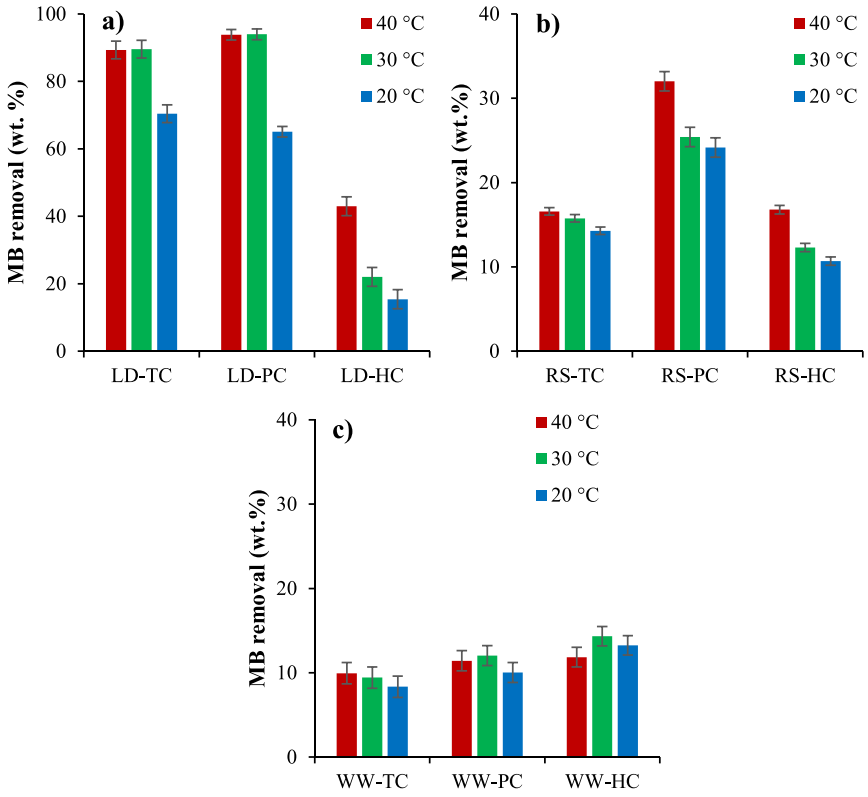

Fig. 7. Effects of temperature (20–40 °C) on MB removal efficiencies of a) LD-based biochars, b) RS-based biochars, and c) WW-based biochars under 200 ppm of initial MB concentration for 24 h.

noted for RS and WW. The MB removal and adsorption capacity isotherms of RS- and WW-based biochars at different initial MB concentrations (50–200 ppm) at 30 °C for 60 min are presented in Supplementary Fig. S4. Based on the results of this study, a solution concentration of 200 ppm was used for all subsequent tests.

3.4.2. *pH of MB solution*

pH solutions from 2 to 10 were tested for a 200 ppm MB dye solution to assess the influence of pH on MB uptake for the different biochars. The results of the pH illustrated that the biochars demonstrated relatively low adsorption capacities at the strong acidic environments (Fig. 6) However, the removal remained at constant rates between the pH levels of 4–10 for all samples, which is similar to previous studies [48,89]. The mechanism of biochar dye adsorption is a combination of electrostatic interaction, hydrogen bonding, functional group interaction, and Van der Wal forces [8]. MB dye is a cationic dye, and thus higher pH is favoured. This is because a higher pH increases the presence of OH^- ions, which in turn makes the surface of biochar negative, which promotes the electrostatic attraction between the positively charged cationic dye and the negatively charged biochar surface. The biochars in this study were not activated to enhance their adsorption as the study aimed to assess their potential as biochars without further processing. Based on this study a pH of 6 was selected for all further tests to ensure optimal adsorptions for all biochars.

3.4.3. *Adsorption temperature*

Three different solution temperatures (20, 30 and 40 °C) were tested using a 200 ppm MB dye solution to assess the impact of temperature on the MB uptake of the different biochars. Fig. 7 illustrates that lower temperatures exhibited lower uptakes for all samples, which is in line

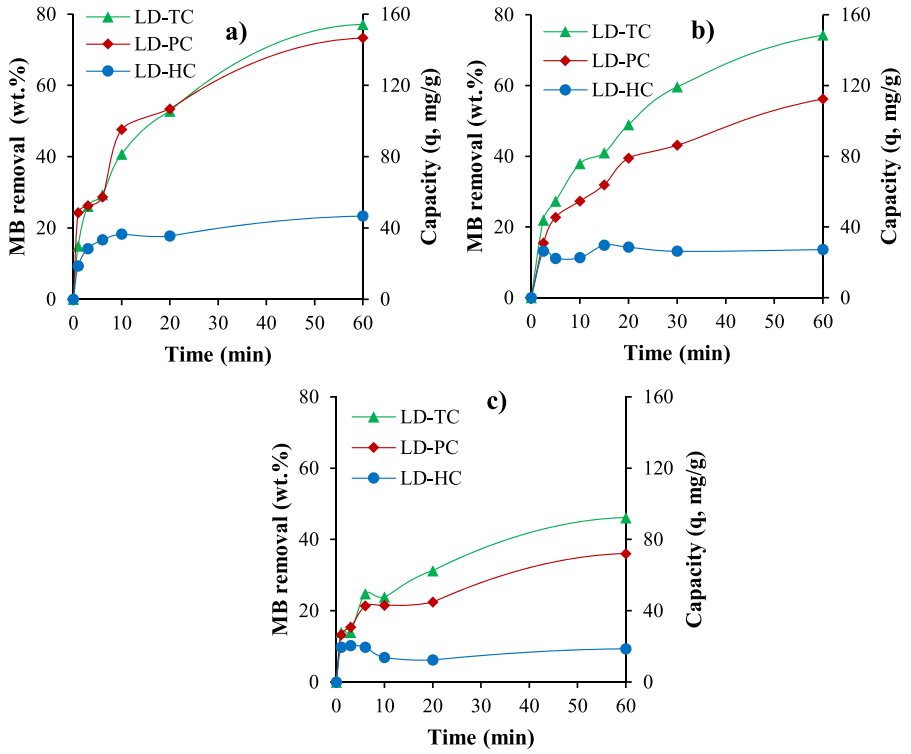

Fig. 8. MB removal and adsorption capacity isotherms of LD-based biochars at different temperatures a) 40 °C, b) 30 °C and c) 20 °C under initial MB concentration of 200 ppm for 60 min.

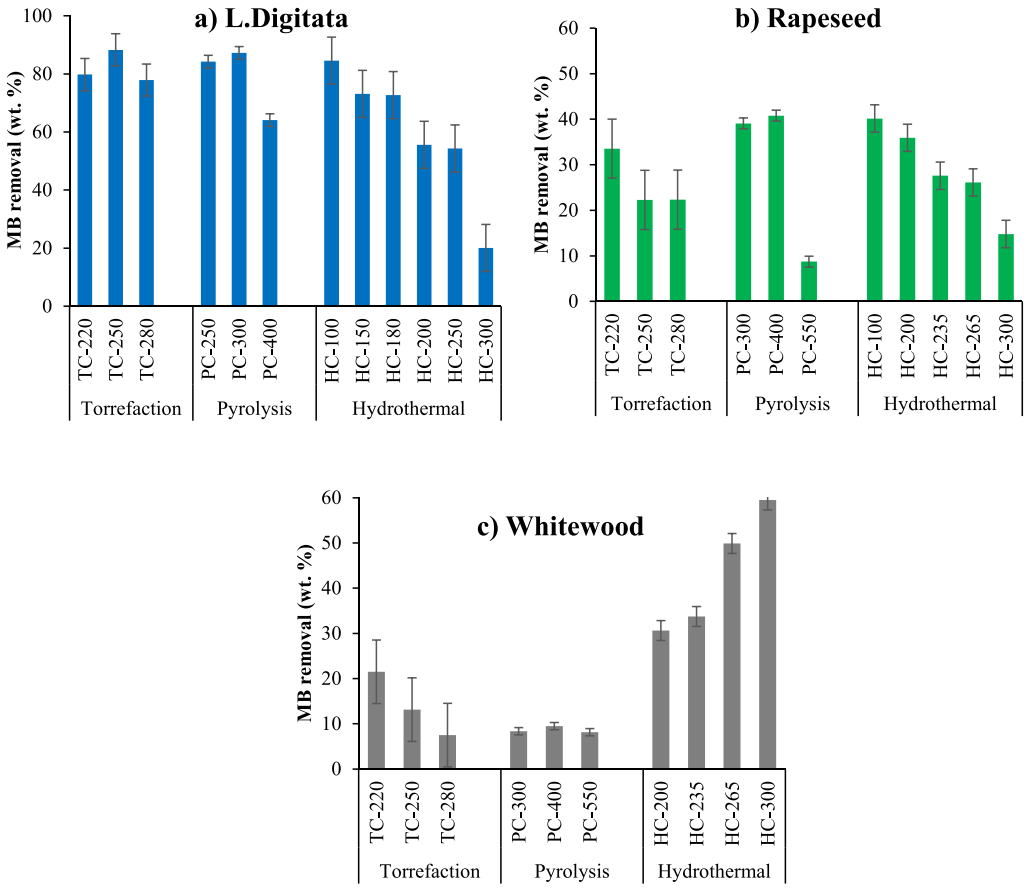

Fig. 9. MB removal efficiency of biochars produced by hydrothermal conversion (HC), pyrolysis (PC), and torrefaction (TC) at 100 ppm of initial MB concentration at 30 °C.

with previous studies [49,90]. MB removal and adsorption capacity isotherms of LD- based biochars at different temperatures (40–20 °C) under 200 ppm of initial MB concentration for 60 min are presented in Fig. 8, and MB removal and adsorption capacity isotherms of RS- and WW-based biochars (Supplementary Fig. S5). LD had the highest MB dye uptake rates, with pyrolysis biochars adsorbing ~ 94 wt% MB dye (~160 mg/g) at 30 and 40 °C dye solution respectively (Fig. 7a and 8a). Slightly lower uptakes were observed for torrefied LD biochars at 30 °C and 40 °C (~89 wt% MB dye (115–150 mg/g) adsorption), while the hydrothermal LD biochars only adsorbed ~ 43 wt% (40 mg/g) at 40 °C dye solution temperature (Fig. 7a and 8a).

LD biochars had higher surface area and pore volume than the than the pyrolysis and torrefied LD biochars (Fig. 2), indicating that the uptake is not directly related to surface area or pore volume. The FTIR analysis (Fig. 3) shows that some functional groups disappeared for hydrothermal processing temperatures over 180 °C. The functional group can absorb MB dye via electrostatic attraction, cation exchange and surface complex mechanisms [91]. Torrefaction did not significantly change the FTIR profile (Fig. S3), indicating that the functional groups were unaffected due to this processing technique and did not interfere with the adsorption mechanisms. WW had the lowest MB dye adsorption rates for all thermal processing routes, with adsorption never reaching above ~ 15 wt% (<30 mg/g) (Fig. 7c and Fig. S5). RS exhibited relatively low adsorption rates (<30 wt%), but with large variances between the thermal processing techniques (Fig. 7b). As for LD, pyrolysis produced the highest adsorption rates for RS, with increasing temperature having a clear influence on enhancing uptake. Torrefaction and hydrothermal processing both resulted in similar uptake rates for RS.

3.5. MB removal capacities of the biochars

Fig. 9. shows the MB removal efficiencies for the biochars produced from LD, RS, and WW. Fig. 9a. shows that the removal efficiencies (~77–87 wt%) of biochars produced from LD via torrefaction did not show significant differences. Similarly, the LD biochars produced via pyrolysis at 250–300 °C provide a relatively high removal capacities (84–87 wt%), while the removal efficiency decreases to 64 wt% for the LD biochar produced at higher temperatures 400 °C (Fig. 9a). The high MB adsorption capacity of the biochars produced via torrefaction and low temperature pyrolysis (250–300 °C) could be attributed to the surface functional groups, which did not significantly change via torrefaction, low temperature pyrolysis. The biochars produced form LD with hydrothermal conversion at lower temperature provide higher MB adsorption capacities (Fig. 9a) even though the biochars produced at those temperatures provide lower surface area and micro pore volume. However, the MB removal capacity of the biochars produced from RS via torrefaction (<33 wt%), pyrolysis (<40 wt%), and hydrothermal conversion (<35 wt%) is relatively low compared to that of the biochars produced from LD (Fig. 9b.). Compared to other biomass feedstocks, WW had the lowest MB removal capacity (~18 wt% in Fig. 9c). The biochars produced from WW via torrefaction and pyrolysis also provided relatively low MB removal capacities, < 20 wt% and < 10 wt%, respectively. However, unlike the biochars produced from RS and LD, WW-based biochars (produced via hydrothermal conversion at higher temperature) provide the highest MB removal capacity i.e. reaching ~ 60 wt% for the biochar produced at 300 °C in hydrothermal conversion (Fig. 9c).

3.6. Kinetics and equilibrium models

3.6.1. Adsorption kinetics

Based on the results presented in the Section 3.4 and 3.5, LD-based biochars produced with torrefaction and pyrolysis exhibited the greatest potential to be used as an adsorbent for MB dye. RS-based biochars produced with pyrolysis and hydrothermal conversion at low temperatures also showed reasonable level of MB removal. However, WW-based biochars demonstrated relatively low MB removal compared to LD- and RS-based biochars. Therefore, the adsorption kinetics were only evaluated for the potential biochars (LD- and RS-based biochars) using Pseudo-first order, Pseudo-second order, and Intra-particle diffusion models. The adsorption rate constants (k1.ad, k2.ad, and k3.ad) and theoretical equilibrium uptake capacities ($q_{eq.cal}$) of each adsorbent for the Pseudo-first order, Pseudo-second order, and Intra-particle diffusion models are presented in Table 2. The mean absolute percentage error (ε, MAPE) and the correlation coefficients (R^2) for pseudo-second-order kinetic were much lower than those with the pseudo-first order and Intra-particle diffusion kinetic models (Table 2), which is similar to previous findings [53]. The MB adsorption kinetics for biochars and comparison of estimated adsorption capacities by Pseudo-second order with experimental results are presented in Figs. 10 and 11 for LD- and RS-based biochars produced by torrefaction and pyrolysis (Fig. S6 present for the biochars produced by hydrothermal conversion). These results demonstrated that the pseudo-second order kinetic model fits and identify the adsorption kinetics of MB onto the sorbents (LD- and RS-based biochars). This confirms that the adsorption of MB might be controlled by multiple processes involving electrostatic attraction, ion exchange, complexation, and surface deposition [92].

Table 2
Comparison of the experimental and estimated q_{eq} values for the pseudo-first order and pseudo-second order adsorption kinetics at 100 ppm of initial MB concentration.

Adsorbents	L. digitata			Rapeseed		
	LD-TC	LD-PC	LD-HC	RS-TC	RS-PC	RS-HC
$q_{eq.exp}$ (mg/g)	88.3	87.3	29.9	9.1	32.9	9.3
Pseudo-first order						
$q_{eq.cal}$ (mg/g)	84.2	62.0	20.0	9.3	22.0	6.6
k1.ad (1/min)	0.092	0.059	0.026	0.501	0.072	0.067
R^2	0.969	0.976	0.967	0.97	0.974	0.862
ε* (%)	4.6	>10	>10	2.7	>10	>10
Pseudo-second order						
$q_{eq.cal}$ (mg/g)	96.2	91.7	31.3	9.3	34.0	9.5
k2.ad (g/mg. min)	0.002	0.002	0.005	0.073	0.014	0.072
R^2	0.979	0.984	0.984	0.996	0.997	0.998
ε* (%)	4.1	5.1	4.5	2.2	3.3	2.2
Intra-particle diffusion						
C	6.61	13.82	3.96	3.13	8.27	3.05
k3.ad (mg/g. $min^{1/2}$)	12.054	13.824	3.407	1.048	4.043	1.049
R^2	0.916	0.915	0.939	0.538	0.775	0.689

*ε is the mean absolute percentage error (MAPE). The abbreviations: "HC", "PC" and "TC", represent the biochars produced by hydrothermal conversion, pyrolysis, and torrefaction, respectively.

3.6.2. Adsorption equilibrium models

The adsorption equilibrium and maximum adsorption capacity of LD- and RS-based biochars were fitted to Langmuir and Freundlich adsorption isotherms and the results presented in Fig. 12. The parameters of Langmuir and Freundlich adsorption isotherms were determined based on their linearised equations (Eq-8 and Eq-10) and presented in Table 3. Based on the Eq-8 (for the Langmuir adsorption model), a plot of $1/q_{eq}$ vs $1/C_{eq}$ gives a straight line with a slope of Q^0 (maximum amount of adsorbent adsorbed per gram of adsorbent), and an intercept of b (free energy of adsorbent). Based on the Eq-10 (for the Freundlich adsorption model), a linear plot of log q_{eq} vs log C_{eq} provides the n (adsorption intensity) and K_F (adsorption capacity) using the slope and the intercept of the graph, respectively. Fig. 12 and Table 3 show that the MB adsorption results of LD-based biochars produced with torrefaction and pyrolysis have a better fit with the Langmuir model, as they have higher correlation coefficients and lower mean absolute

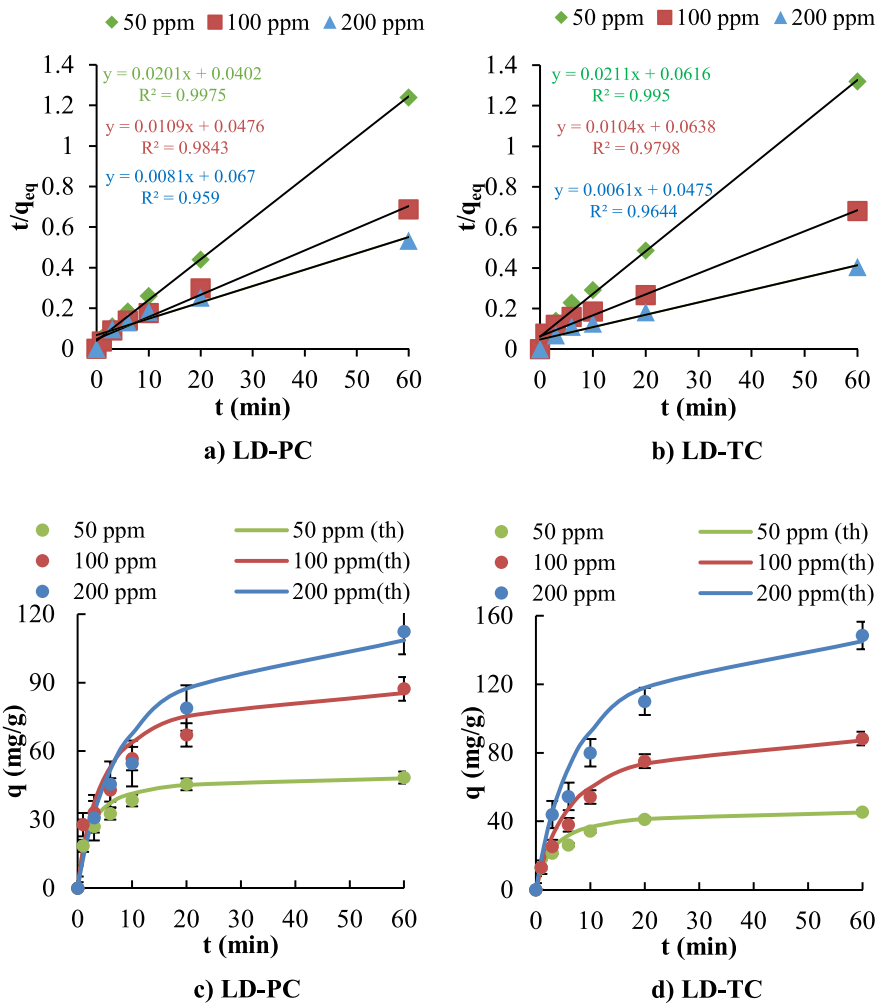

Fig. 10. Pseudo-second order adsorption kinetics of MB (a-b) and comparison of estimated adsorption capacities by Pseudo-second order with experimental results (c-d). LD-PC (a, c), LD-TC (b, d).

percentage errors). Thus, the adsorbent surface can be assumed to be energetically homogeneous [53], which agrees with other publications on MB removal with green macro alga Caulerpa lentillifera [56].

However, the biochar produced from LD with hydrothermal conversion showed a better fit with the Freundlich model, which indicates the MB dye adsorption occurred on the heterogeneous surface [40]. RS-based biochars (produced by torrefaction, pyrolysis and hydrothermal conversion) demonstrate a better fit with the Freundlich adsorption equilibrium model. In the Freundlich adsorption models, the magnitude of "n" could identify the excellence of adsorption, where an "*n*" value <1.0 indicates poor adsorption characteristics [53]. All adsorbents in this study had *n* values over 1, indicating they have good adsorption characteristics. Table 3 demonstrated that the maximum saturated adsorption capacity (Q^0) of the biochars produced from LD with torrefaction (LD-TC-250) and pyrolysis (LD-PC-400) are relatively high (175 mg/g and 117 mg/g, respectively). Furthermore, the RS biochar produced by pyrolysis (RS-PC-400) also demonstrated a reasonable amount of maximum adsorption capacity at 71 mg/g.

3.6.3. *Adsorption thermodynamics*

The slope and intercept of the straight line in the plot of lnK_d vs $1/T$ (Van't Hoff plot) gives the standard enthalpy ($\Delta H^\circ/R$) and standard entropy ($\Delta S^\circ/R$) of the kinetic data, respectively [93]. The Van't Hoff plots for the RS, LD, WW, and biochars are presented in Supplementary (Fig. S8-S10). The thermodynamic parameters (ΔH°, ΔS°, and ΔG°) are determined using the Van't Hoff plots and the results for RS- and LD-based biochars are presented in Table 4. The biochars produced from RS and LD showed a positive ΔH° values indicating an endothermic adsorption [42]. Only WW-HC (biochar produced by hydrothermal conversion) provided a negative ΔH° (-9.26 kj/mol) while the rest of the WW-based biochars showed positive ΔH° values (Table 4). The level of ΔH° can also provide further information about adsorption mechanisms. The ΔH° is in the range of 40–200 kJ/mol in the chemical bonds resulted from chemical adsorption [90]. However, when $\Delta H^\circ < 25$ kJ/mol, the acting force is Van der Waals' force, and this could be attributed to physical adsorption [90].

In this study, MB adsorption onto biochars produced from LD was driven by chemical adsorption, while physical adsorption was predominant for the other sorbents. The ΔH° value for RS-PC was in the middle of physisorption and chemisorption, and thus the process could be identified as a physical adsorption enhanced by a chemical effect. Positive ΔS° values were observed for the biochars produced from RS and LD, which indicates the affinity of adsorbent for MB [42] and an increase in the randomness at the interface adsorbent/adsorbate during adsorption [55,71]. As for the Gibbs free energy, RS-based biochars demonstrated positive ΔG° values at different temperatures and the values decreased in the following order 0 < RS-PC < RS-TC < RS-HC, which means biochar produced from RS are not suitable for MB adsorption. However, a negative ΔG° values were observed for the LD-TC < LD-PC < 0, which indicates that the MB removal could be a thermodynamically favourable process due to the spontaneous nature of the adsorption [55,71]. This explains the higher MB adsorption capacities of LD-TC,

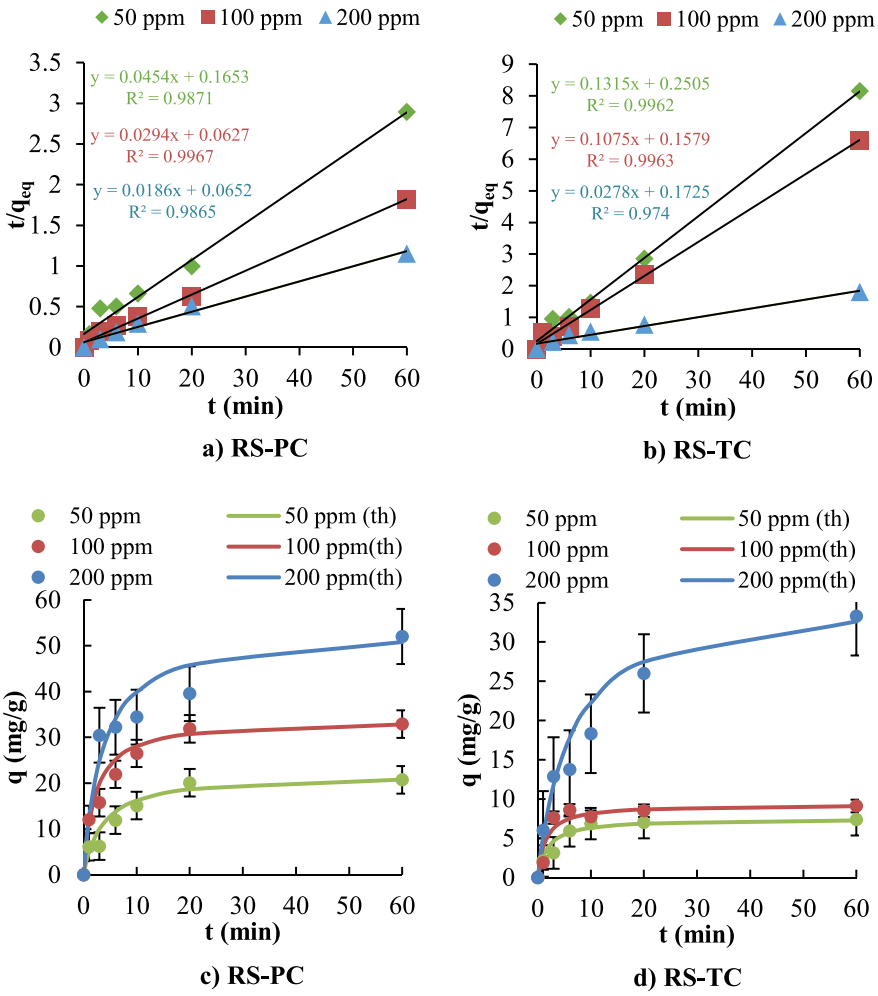

Fig. 11. Pseudo-second order adsorption kinetics of MB (a-b) and comparison of estimated adsorption capacities by Pseudo-second order with experimental results (c-d). RS-PC (a, c), RS-TC (b, d).

and LD-PC compared to RS-based and WW-based biochars. Furthermore, the decrease in the ΔG° values for LD-based biochars with increasing the adsorption temperature suggest that the process increases in spontaneity at higher temperature [71] and the adsorption becomes more favourable with increasing temperature [55].

3.7. Performance assessment of biochars with literature

The adsorption capacities of the most promising biochars (produced from LD via torrefaction and pyrolysis and RS via pyrolysis) for the adsorption of MB has been compared with the other biochars reported in the literature (Table 5). By comparison of the MB removal results in this study with those presented in previous research, LD-biochars produced by torrefaction (LD-TC-250) and pyrolysis (LD-PC-400), and RS-biochars produced by pyrolysis (RS-PC-400) provide relatively promising MB adsorption capacities compared to the adsorption capacities of biochars derived a wide range of biomass feedstocks presented in Table 5. The comparison results show that the LD-based and RS-based biochars are competitive for the application of MB-removal from wastewater.

4. Conclusions

This research reports an extensive comparative study on how the biomass processing pathways (torrefaction, pyrolysis, and hydrothermal conversion) and process interdependencies are influenced by different feedstocks (WW, RS, and LD) for the optimisation of biochar formation and their associated wastewater treatment (removal of MB) applications.

Based on the comparative evaluation of biomass feedstocks and biochar in MB removal,

- LD-based biochars produced with torrefaction (LD-TC) and pyrolysis (LD-PC) exhibited the greatest potential to be used as an adsorbent for MB dye (~175 mg/g for LD-TC and ~ 117 mg/g for LD-PC).
- RS-based biochars produced with pyrolysis (RS-PC) showed reasonable level of MB removal (~71 mg/g for RS-PC), however, the biochars produced with hydrothermal conversion and torrefaction showed relatively lower MB removal.
- WW-based biochars demonstrated the lowest MB adsorption capacities (<30 mg/g).
- The MB adsorption results onto LD- and RS-based biochars fit well with the Pseudo-second-order kinetic model.
- The adsorption process was described well by the Langmuir isotherms for LD-based biochars and by Freundlich adsorption isotherm for RS-based biochars.
- Based on the thermodynamic analysis, the MB removal by LD-based biochars (LD-TC and LD-PC) could be a thermodynamically favourable process as a result of a negative Gibbs free energy (ΔG°), which indicates MB adsorption on these biochars is spontaneous and physical in nature.

This study provides a clear understanding on how the optimal

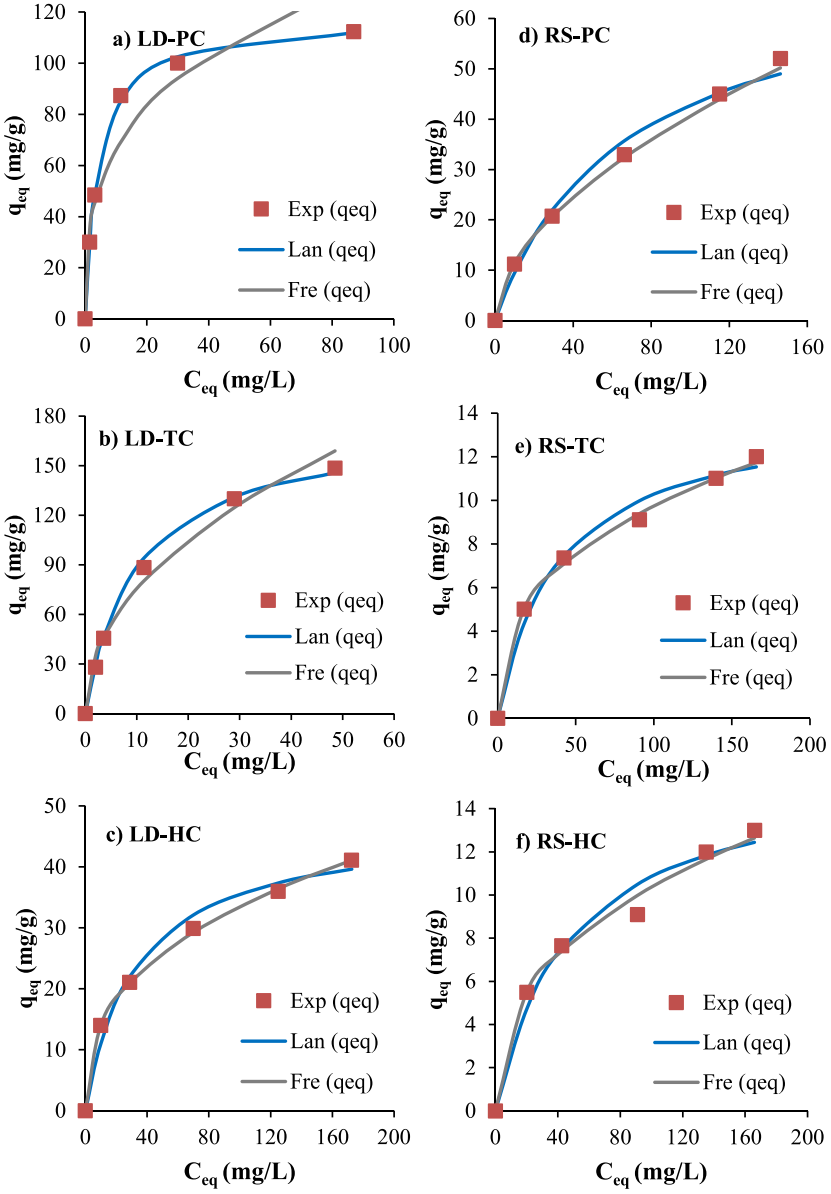

Fig. 12. Experimental and estimated non-linearized adsorption isotherms of MB on LD-based biochars; a) LD-PC, b) LD-TC, c) LD-HC, and RS-based biochars; d) RS-PC, e) RS-TC, f) RS-HC. ("Exp", "Lan", and "Fre" are the q_{eq} values determined by experimental, Langmuir Model, and Freundlich Model, respectively).

Table 3
The parameters of adsorption isotherms in Langmuir and Freundlich models.

Adsorbents	Langmuir Model				Freundlich Model			
	Q^o(mg/g)	b	R^2	ε* (%)	K_F	n	R^2	ε* (%)
LD-TC	175.8	0.102	0.995	3.2	25.5	2.12	0.990	5.6
LD-PC	117.6	0.226	0.999	1.5	31.4	3.10	0.903	>10
LD-HC	47.1	0.030	0.987	4.8	5.6	2.66	0.999	1.0
RS-TC	14.2	0.025	0.982	4.0	1.76	2.69	0.994	2.3
RS-PC	70.9	0.015	0.980	5.1	3.17	1.80	0.999	2.1
RS-HC	16.1	0.020	0.953	5.7	1.69	2.53	0.978	4.6

*ε is the mean absolute percentage error (MAPE). The unit of K_F is (mg/g)(mg/L)^n.

holistic biomass processing pathways and process interdependencies influence the MB dye adsorption properties of biochars made from three distinctly different biomass feedstocks. As future work, an optimisation study based on particle size, pH, expended MB concentration, adsorption temperature using the most promising biochars (provided in this study) can be experimentally performed to understand the maximum capacity of these biochars under optimised conditions. Additionally, based on this extensive research, an artificial intelligence model and statistical analysis into the wastewater treatment of biochars can be developed to predict the adsorption capacities for the potential other experimental conditions.

Table 4
Thermodynamic parameters for MB adsorption onto RS, LD, WW, and biochars (200 ppm of MB solution at 20, 30, 40 °C).

Adsorbents	Process	ΔH°	ΔS°	ΔG°_{298K}	ΔG°_{303K}	ΔG°_{313K}
		kJ/mol	kJ/mol K	kJ/mol	kJ/mol	kJ/mol
LD-TC	Torrefaction	89.53	0.305	**−0.067**	**−3.125**	**−6.183**
LD-PC	Pyrolysis	61.27	0.205	1.075	**−0.978**	**−3.033**
LD-HC	Hydrothermal	41.63	0.123	5.534	4.302	3.070
RS-TC	Torrefaction	6.61	0.007	4.356	4.279	4.202
RS-PC	Pyrolysis	33.96	0.102	3.845	2.817	1.789
RS-HC	Hydrothermal	4.65	−0.001	5.212	5.231	5.250
WW-TC	Torrefaction	5.77	0.000	5.721	5.719	5.718
WW-PC	Pyrolysis	8.64	0.011	5.477	5.369	5.261
WW-HC	Hydrothermal	**−9.26**	−0.045	4.203	4.662	5.122

Table 5
Comparison of the maximum MB adsorption capacities of biomass and biochars.

Source for biochar	Biochar preparation method	Capacity (mg/g)	Reference
Banana peel extract	Pyrolysis (600 °C, 60 min)	40.19	[48]
Cottonwood	Pyrolysis (600 °C, 60 min)	8.0	[94]
Sewage-sludge	Pyrolysis (550 °C, 2 h)	29.85	[90]
Wheat straw	Pyrolysis (550 °C, 5 min)	12.03	[43]
MMDM	Pyrolysis (300 °C, 12 h)	7.2	[41]
Reed straw biomass	Pyrolysis (500 °C, 2 h)	4.8	[89]
Citrus waste	Hydrothermal (180 – 250 °C)	51.0–17.9	[91]
Winery waste	Hydrothermal (180 – 250 °C)	36.6–22.5	[25]
Mixed tea waste sewage sludge	Pyrolysis (300 °C, 2 h)	8.94	[95]
Municipal solid waste	Pyrolysis (400–500 °C, 15 min)	21.83	[39]
Pumpkin peel	Pyrolysis (250 °C, 60 min)	80.78	[37]
Reeds	Pyrolysis (500 °C, 2 h)	48.84	[38]
Palm bark	Pyrolysis (400 °C, 30 min)	1.21	[96]
Anaerobic digestion residue	Pyrolysis (400 °C, 30 min)	1.69	[96]
L. Digitata	Torrefaction (250 °C, 60 min)	148.5* (175)	In this study
L. Digitata	Pyrolysis at (400 °C, 60 min)	112.3* (117)	In this study
Rapeseed residue	Pyrolysis at (400 °C, 60 min)	56.2* (71)	In this study

*Adsorption capacities in a concentration of 200 ppm of MB solution at 30 °C. The values in brackets are the maximum adsorption capacity determined by Langmuir model.

CRediT authorship contribution statement

Fatih Güleç: Conceptualization, Formal analysis, Methodology, Investigation, Validation, Visualization, Writing – original draft, Writing – review & editing. **Orla Williams:** Conceptualization, Funding acquisition, Methodology, Supervision, Writing – original draft, Writing – review & editing. **Emily T. Kostas:** Methodology, Funding acquisition, Writing – review & editing. **Abby Samson:** Methodology, Funding acquisition, Writing – review & editing. **Lee A. Stevens:** Methodology, Formal analysis. **Edward Lester:** Conceptualization, Methodology, Supervision, Project administration, Funding acquisition, Writing – review & editing.

Declaration of Competing Interest

The authors declare that they have no known competing financial interests or personal relationships that could have appeared to influence the work reported in this paper.

Data availability

Data will be made available on request.

Acknowledgements

This research was funded and supported by the EPSRC & BBSRC UK Supergen Bioenergy Hub [Grant number EP/S000771/1], the University of Nottingham Anne McLaren Research Fellowship (Dr Orla Williams), and the UK Biotechnology and Biological Sciences Research Council (BBSRC) Discovery Fellowship (Dr Emily Kostas) [Grant number BB/S010610/1]. We also would like to acknowledge Dr David Gray, Dr Filippo Bramante, and Dr Vincenzo Di Bari for supplying Rapeseed for this project and Dr David Furniss for his support with the FTIR analyses.

Appendix A. Supplementary data

Supplementary data to this article can be found online at https://doi.org/10.1016/j.fuel.2022.125428.

References

[1] Liang L, Xi F, Tan W, Meng X, Hu B, Wang X. Review of organic and inorganic pollutants removal by biochar and biochar-based composites. Biochar 2021;3(3):255–81.
[2] Kumar M, Oyedun AO, Kumar A. A review on the current status of various hydrothermal technologies on biomass feedstock. Renew Sustain Energy Rev 2018;81:1742–70.
[3] Kostas ET, Williams OSA, Duran-Jimenez G, Tapper AJ, Cooper M, Meehan R, et al. Microwave pyrolysis of Laminaria digitata to produce unique seaweed-derived bio-oils. Biomass Bioenergy 2019;125:41–9.
[4] Qiu B, Tao X, Wang H, Li W, Ding X, Chu H. Biochar as a low-cost adsorbent for aqueous heavy metal removal: a review. J Anal Appl Pyrol 2021;155:105081.
[5] Nhuchhen DR, Basu P, Acharya B. A comprehensive review on biomass torrefaction. Int J Renew Energy Biofuels 2014;2014:1–56.
[6] Pohlmann JG, Osório E, Vilela AC, Diez MA, Borrego AG. Integrating physicochemical information to follow the transformations of biomass upon torrefaction and low-temperature carbonization. Fuel 2014;131:17–27.
[7] Dai Y, Zhang N, Xing C, Cui Q, Sun Q. The adsorption, regeneration and engineering applications of biochar for removal organic pollutants: a review. Chemosphere 2019;223:12–27.
[8] Srivatsav P, Bhargav BS, Shanmugasundaram V, Arun J, Gopinath KP, Bhatnagar A. Biochar as an eco-friendly and economical adsorbent for the removal of colorants (dyes) from aqueous environment: A review. Water 2020;12(12):3561.
[9] Güleç F, Özdemir GDT. Investigation of drying characteristics of Cherry Laurel (Laurocerasus officinalis Roemer) fruits. Akademik ziraat dergisi 2017;6(1):73–80.
[10] Güleç F, Şimşek EH, Sarı HT. Prediction of biomass pyrolysis mechanisms and kinetics–Application of Kalman filter. Chem Eng Technol 2022;45(1):167–77.
[11] Lachos-Perez D, César Torres-Mayanga P, Abaide ER, Zabot GL, De Castilhos F. Hydrothermal carbonization and Liquefaction: differences, progress, challenges, and opportunities. Bioresour Technol 2022;343:126084.
[12] Evcil T, Simsir H, Ucar S, Tekin K, Karagoz S. Hydrothermal carbonization of lignocellulosic biomass and effects of combined Lewis and Brønsted acid catalysts. Fuel 2020;279.
[13] Ruiz HA, Rodríguez-Jasso RM, Fernandes BD, Vicente AA, Teixeira JA. Hydrothermal processing, as an alternative for upgrading agriculture residues and marine biomass according to the biorefinery concept: a review. Renew Sustain Energy Rev 2013;21:35–51.

[14] Alper K, Tekin K, Karagöz S, Ragauskas AJ. Sustainable energy and fuels from biomass: a review focusing on hydrothermal biomass processing. Sustain Energy Fuels 2020;4(9):4390–414.
[15] Güleç F, Riesco LMG, Williams O, Kostas ET, Samson A, Lester E. Hydrothermal conversion of different lignocellulosic biomass feedstocks–Effect of the process conditions on hydrochar structures. Fuel 2021;302:121166.
[16] González-Arias J, Gómez X, González-Castaño M, Sánchez ME, Rosas JG, Cara-Jiménez J. Insights into the product quality and energy requirements for solid biofuel production: A comparison of hydrothermal carbonization, pyrolysis and torrefaction of olive tree pruning. Energy 2022;238:122022.
[17] Atallah E, Zeaiter J, Ahmad MN, Leahy JJ, Kwapinski W. Hydrothermal carbonization of spent mushroom compost waste compared against torrefaction and pyrolysis. Fuel Process Technol 2021;216:106795.
[18] Huff MD, Kumar S, Lee JW. Comparative analysis of pinewood, peanut shell, and bamboo biomass derived biochars produced via hydrothermal conversion and pyrolysis. J Environ Manage 2014;146:303–8.
[19] Pandey D, Daverey A, Arunachalam K. Biochar: Production, properties and emerging role as a support for enzyme immobilization. J Cleaner Prod 2020;255:120267.
[20] Manyà JJ. Pyrolysis for biochar purposes: a review to establish current knowledge gaps and research needs. Environ Sci Technol 2012;46(15):7939–54.
[21] Zhao L, Cao X, Mašek O, Zimmerman A. Heterogeneity of biochar properties as a function of feedstock sources and production temperatures. J Hazard Mater 2013;256:1–9.
[22] Zhao S-X, Ta N, Wang X-D. Effect of temperature on the structural and physicochemical properties of biochar with apple tree branches as feedstock material. Energies 2017;10(9):1293.
[23] Pecha MB, Arbelaez JIM, Garcia-Perez M, Chejne F, Ciesielski PN. Progress in understanding the four dominant intra-particle phenomena of lignocellulose pyrolysis: chemical reactions, heat transfer, mass transfer, and phase change. Green Chem 2019;21(11):2868–98.
[24] Varma AK, Thakur LS, Shankar R, Mondal P. Pyrolysis of wood sawdust: Effects of process parameters on products yield and characterization of products. Waste Manage 2019;89:224–35.
[25] El-Naggar A, El-Naggar AH, Shaheen SM, Sarkar B, Chang SX, Tsang DCW, et al. Biochar composition-dependent impacts on soil nutrient release, carbon mineralization, and potential environmental risk: a review. J Environ Manage 2019;241:458–67.
[26] Mohan D, Abhishek K, Sarswat A, Patel M, Singh P, Pittman CU. Biochar production and applications in soil fertility and carbon sequestration–a sustainable solution to crop-residue burning in India. RSC Adv 2018;8(1):508–20.
[27] Güleç F. Demonstrating the applicability of chemical looping combustion for fluid catalytic cracking unit as a novel CO2 capture technology. Chemical Engineering. PhD: University of Nottingham; 2020.
[28] Mamvura TA, Danha G. Biomass torrefaction as an emerging technology to aid in energy production. Heliyon 2020;6(3):e03531.
[29] Scarlat N, Dallemand J, Taylor N, Banja M, Sanchez Lopez J, Avraamides M. Brief on biomass for energy in the European Union. Luxembourg: Publications Office of the European Union; 2019.
[30] Román S, Nabais JMV, Laginhas C, Ledesma B, González JF. Hydrothermal carbonization as an effective way of densifying the energy content of biomass. Fuel Process Technol 2012;103:78–83.
[31] Kopac T. Hydrogen storage characteristics of bio-based porous carbons of different origin: A comparative review. Int J Energy Res 2021;45(15):20497–523.
[32] Güleç F, Williams O, Kostas ET, Samson A, Lester E. A comprehensive comparative study on the energy application of chars produced from different biomass feedstocks via hydrothermal conversion, pyrolysis. and torrefaction. The University of Nottingham; 2022.
[33] Güleç F, Samson A, Williams O, Kostas ET, Lester E. Biofuel characteristics of chars produced from rapeseed, whitewood, and seaweed via thermal conversion technologies – Impacts of feedstocks and process conditions. The University of Nottingham; 2022.
[34] Osman AI, Mehta N, Elgarahy AM, Al-Hinai A. Ala'a H, Rooney DW. Conversion of biomass to biofuels and life cycle assessment: A review. Environmental Chemistry Letters; 2021. p. 1–44.
[35] Yener J, Kopac T, Dogu G, Dogu T. Batch adsorber rate analysis of Methylene Blue on Amberlite and Clinoptilolite. Sep Sci Technol 2006;41(9):1857–79.
[36] Yener J, Kopac T, Dogu G, Dogu T. Dynamic analysis of sorption of Methylene Blue dye on granular and powdered activated carbon. Chem Eng J 2008;144(3):400–6.
[37] Rashid J, Tehreem F, Rehman A, Kumar R. Synthesis using natural functionalization of activated carbon from pumpkin peels for decolourization of aqueous methylene blue. Sci Total Environ 2019;671:369–76.
[38] Wang Y, Zhang Y, Li S, Zhong W, Wei W. Enhanced methylene blue adsorption onto activated reed-derived biochar by tannic acid. J Mol Liq 2018;268:658–66.
[39] Sumalinog DAG, Capareda SC, de Luna MDG. Evaluation of the effectiveness and mechanisms of acetaminophen and methylene blue dye adsorption on activated biochar derived from municipal solid wastes. J Environ Manage 2018;210:255–62.
[40] Jawad AH, Abdulhameed AS, Mastuli MS. Acid-factionalized biomass material for methylene blue dye removal: a comprehensive adsorption and mechanism study. J Taibah Univ Sci 2020;14(1):305–13.
[41] Hoslett J, Ghazal H, Mohamad N, Jouhara H. Removal of methylene blue from aqueous solutions by biochar prepared from the pyrolysis of mixed municipal discarded material. Sci Total Environ 2020;714:136832.
[42] Bulut Y, Aydın H. A kinetics and thermodynamics study of methylene blue adsorption on wheat shells. Desalination 2006;194(1–3):259–67.
[43] Liu Y, Zhao X, Li J, Ma D, Han R. Characterization of bio-char from pyrolysis of wheat straw and its evaluation on methylene blue adsorption. Desalin Water Treat 2012;46(1–3):115–23.
[44] Sen TK, Afroze S, Ang H. Equilibrium, kinetics and mechanism of removal of methylene blue from aqueous solution by adsorption onto pine cone biomass of Pinus radiata. Water Air Soil Pollut 2011;218(1):499–515.
[45] Özer D, Dursun G, Özer A. Methylene blue adsorption from aqueous solution by dehydrated peanut hull. J Hazard Mater 2007;144(1–2):171–9.
[46] Vadivelan V, Kumar KV. Equilibrium, kinetics, mechanism, and process design for the sorption of methylene blue onto rice husk. J Colloid Interface Sci 2005;286(1):90–100.
[47] Rubin E, Rodriguez P, Herrero R, Cremades J, Barbara I, Sastre de Vicente ME. Removal of methylene blue from aqueous solutions using as biosorbent Sargassum muticum: an invasive macroalga in Europe. J Chem Technol Biotechnol Int Res Process Environ Clean Technol 2005;80(3):291–8.
[48] Zhang P, O'Connor D, Wang Y, Jiang L, Xia T, Wang L, et al. A green biochar/iron oxide composite for methylene blue removal. J Hazard Mater 2020;384:121286.
[49] Yao X, Ji L, Guo J, Ge S, Lu W, Cai Lu, et al. Magnetic activated biochar nanocomposites derived from wakame and its application in methylene blue adsorption. Bioresour Technol 2020;302:122842.
[50] Minisy IM, Salahuddin NA, Ayad MM. Adsorption of methylene blue onto chitosan–montmorillonite/polyaniline nanocomposite. Appl Clay Sci 2021;203:105993.
[51] Oladoja N, Aboluwoye C, Oladimeji Y, Ashogbon A, Otemuyiwa I. Studies on castor seed shell as a sorbent in basic dye contaminated wastewater remediation. Desalination 2008;227(1–3):190–203.
[52] Rafatullah M, Sulaiman O, Hashim R, Ahmad A. Adsorption of methylene blue on low-cost adsorbents: a review. J Hazard Mater 2010;177(1–3):70–80.
[53] Miraboutalebi SM, Nikouzad SK, Peydayesh M, Allahgholi N, Vafajoo L, McKay G. Methylene blue adsorption via maize silk powder: kinetic, equilibrium, thermodynamic studies and residual error analysis. Process Saf Environ Prot 2017;106:191–202.
[54] Senthil Kumar P, Fernando PSA, Ahmed RT, Srinath R, Priyadharshini M, Vignesh AM, et al. Effect of temperature on the adsorption of methylene blue dye onto sulfuric acid–treated orange peel. Chem Eng Commun 2014;201(11):1526–47.
[55] Yagub MT, Sen TK, Ang H. Equilibrium, kinetics, and thermodynamics of methylene blue adsorption by pine tree leaves. Water Air Soil Pollut 2012;223(8):5267–82.
[56] Marungrueng K, Pavasant P. High performance biosorbent (Caulerpa lentillifera) for basic dye removal. Bioresour Technol 2007;98(8):1567–72.
[57] Sahu S, Pahi S, Tripathy S, Singh SK, Behera A, Sahu UK, et al. Adsorption of methylene blue on chemically modified lychee seed biochar: Dynamic, equilibrium, and thermodynamic study. J Mol Liq 2020;315:113743.
[58] Maurya NS, Mittal AK, Cornel P, Rother E. Biosorption of dyes using dead macro fungi: effect of dye structure, ionic strength and pH. Bioresour Technol 2006;97(3):512–21.
[59] De Chirico S, di Bari V, Romero Guzmán MJ, Nikiforidis CV, Foster T, Gray D. Assessment of rapeseed oil body (oleosome) lipolytic activity as an effective predictor of emulsion purity and stability. Food Chem 2020;316:126355.
[60] De Chirico S, di Bari V, Foster T, Gray D. Enhancing the recovery of oilseed rape seed oil bodies (oleosomes) using bicarbonate-based soaking and grinding media. Food Chem 2018;241:419–26.
[61] Kostas ET, White DA, Cook DJ. Development of a bio-refinery process for the production of speciality chemical, biofuel and bioactive compounds from Laminaria digitata. Algal Res 2017;28:211–9.
[62] Williams O, Newbolt G, Eastwick C, Kingman S, Giddings D, Lormor S, et al. Influence of mill type on densified biomass comminution. Appl Energy 2016;182:219–31.
[63] Güleç F, Meredith W, Sun C-G, Snape CE. Demonstrating the applicability of chemical looping combustion for the regeneration of fluid catalytic cracking catalysts. Chem Eng J 2020;389:124492.
[64] Güleç F, Erdogan A, Clough PT, Lester E. Investigation of the hydrodynamics in the regenerator of fluid catalytic cracking unit integrated by chemical looping combustion. Fuel Process Technol 2021;223:106998.
[65] Güleç F, Meredith W, Sun C-G, Snape CE. A novel approach to CO2 capture in fluid catalytic cracking—chemical looping combustion. Fuel 2019;244:140–50.
[66] Güleç F, Meredith W, Sun C-G, Snape CE. Selective low temperature chemical looping combustion of higher alkanes with Cu-and Mn-oxides. Energy 2019;173:658–66.
[67] Güleç F, Pekaslan D, Williams O, Lester E. Predictability of higher heating value of biomass feedstocks via proximate and ultimate analyses–A comprehensive study of artificial neural network applications. Fuel 2022;320:123944.
[68] Kostas ET, Durán-Jiménez G, Shepherd BJ, Meredith W, Stevens LA, Williams OSA, et al. Microwave pyrolysis of olive pomace for bio-oil and bio-char production. Chem Eng J 2020;387:123404.
[69] Karaman C, Aksu Z. Modelling of Remazol Black-B adsorption on chemically modified waste orange peel: pH shifting effect of acidic treatment. Sakarya Üniversitesi Fen Bilimleri Enstitüsü Dergisi 2020;24(5):1127–42.
[70] Karaman C, Karaman O, Show P-L, Orooji Y, Karimi-Maleh H. Utilization of a double-cross-linked amino-functionalized three-dimensional graphene networks as a monolithic adsorbent for methyl orange removal: equilibrium, kinetics, thermodynamics and artificial neural network modeling. Environ Res 2021;112156.
[71] Williams O, Clark I, Gomes RL, Perehinec T, Hobman JL, Stekel DJ, et al. Removal of copper from cattle footbath wastewater with layered double hydroxide

adsorbents as a route to antimicrobial resistance mitigation on dairy farms. Sci Total Environ 2019;655:1139–49.
[72] Abd El-Latif M, Ibrahim AM, El-Kady M. Adsorption equilibrium, kinetics and thermodynamics of methylene blue from aqueous solutions using biopolymer oak sawdust composite. J Am Sci 2010;6(6):267–83.
[73] Chandra S, Bhattacharya J. Influence of temperature and duration of pyrolysis on the property heterogeneity of rice straw biochar and optimization of pyrolysis conditions for its application in soils. J Cleaner Prod 2019;215:1123–39.
[74] Lester E, Gong M, Thompson A. A method for source apportionment in biomass/coal blends using thermogravimetric analysis. J Anal Appl Pyrol 2007;80(1):111–7.
[75] Carrier M, Auret L, Bridgwater A, Knoetze JH. Using apparent activation energy as a reactivity criterion for biomass pyrolysis. Energy Fuels 2016;30(10):7834–41.
[76] Yang H, Yan R, Chen H, Lee DH, Zheng C. Characteristics of hemicellulose, cellulose and lignin pyrolysis. Fuel 2007;86(12–13):1781–8.
[77] Elliott DC, Biller P, Ross AB, Schmidt AJ, Jones SB. Hydrothermal liquefaction of biomass: developments from batch to continuous process. Bioresour Technol 2015;178:147–56.
[78] Heidari M, Dutta A, Acharya B, Mahmud S. A review of the current knowledge and challenges of hydrothermal carbonization for biomass conversion. J Energy Inst 2019;92(6):1779–99.
[79] Arellanoa O, Flores M, Guerra J, Hidalgo A, Rojas D, Strubinger A. Hydrothermal carbonization (HTC) of corncob and characterization of the obtained hydrochar. Chem Eng 2016;50.
[80] Tekin K, Karagöz S, Bektaş S. A review of hydrothermal biomass processing. Renew Sustain Energy Rev 2014;40:673–87.
[81] Sher F, Yaqoob A, Saeed F, Zhang S, Jahan Z, Klemeš JJ. Torrefied biomass fuels as a renewable alternative to coal in co-firing for power generation. Energy 2020;209:118444.
[82] Özbay N, Uzun BB, Varol EA, Pütün AE. Comparative analysis of pyrolysis oils and its subfractions under different atmospheric conditions. Fuel Process Technol 2006;87(11):1013–9.
[83] Güleç F, Niftaliyeva A, Karaduman A. Selective synthesis of 2, 6-triad dimethylnaphthalene isomers by disproportionation of 2-methylnaphthalene over mesoporous MCM-41. Res Chem Intermed 2018;44(12):7205–18.
[84] Yaman E, Ulusal A, Uzun BB. Co-pyrolysis of lignite and rapeseed cake: a comparative study on the thermal decomposition behavior and pyrolysis kinetics. SN Appl Sci 2021;3(1):1–15.
[85] Huang J, Fu S, Gan L. Chapter 2 - Structure and Characteristics of Lignin. In: Huang J, Fu S, Gan L, editors. Lignin Chemistry and Applications. Elsevier; 2019. p. 25–50.
[86] Salam A, Bashir S, Khan I, Hu H. Biochar production and characterization as a measure for effective rapeseed residue and rice straw management: an integrated spectroscopic examination. Biomass Convers Biorefin 2020:1–10.
[87] Kongwudthiti S, Praserthdam P, Tanakulrungsank W, Inoue M. The influence of Si–O–Zr bonds on the crystal-growth inhibition of zirconia prepared by the glycothermal method. J Mater Process Tech 2003;136(1):186–9.
[88] Fertah M, Belfkira A, Taourirte M, Brouillette F. Extraction and characterization of sodium alginate from Moroccan Laminaria digitata brown seaweed. Arabian J Chem 2017;10:S3707–14.
[89] Li Y, Zhang Y, Zhang Y, Wang G, Li S, Han R, et al. Reed biochar supported hydroxyapatite nanocomposite: Characterization and reactivity for methylene blue removal from aqueous media. J Mol Liq 2018;263:53–63.
[90] Fan S, Wang Y, Wang Z, Tang J, Tang J, Li X. Removal of methylene blue from aqueous solution by sewage sludge-derived biochar: Adsorption kinetics, equilibrium, thermodynamics and mechanism. J Environ Chem Eng 2017;5(1):601–11.
[91] Saha N, Volpe M, Fiori L, Volpe R, Messineo A, Reza MT. Cationic dye adsorption on hydrochars of winery and citrus juice industries residues: Performance, mechanism, and thermodynamics. Energies 2020;13(18):4686.
[92] Xu Q, Liu T, Li L, Liu B, Wang X, Zhang S, et al. Hydrothermal carbonization of distillers grains with clay minerals for enhanced adsorption of phosphate and methylene blue. Bioresour Technol 2021;340:125725.
[93] Zaghouane-Boudiaf H, Boutahala M, Arab L. Removal of methyl orange from aqueous solution by uncalcined and calcined MgNiAl layered double hydroxides (LDHs). Chem Eng J 2012;187:142–9.
[94] Zhang M, Gao B, Yao Y, Xue Y, Inyang M. Synthesis, characterization, and environmental implications of graphene-coated biochar. Sci Total Environ 2012;435:567–72.
[95] Fan S, Tang J, Wang Yi, Li H, Zhang H, Tang J, et al. Biochar prepared from co-pyrolysis of municipal sewage sludge and tea waste for the adsorption of methylene blue from aqueous solutions: kinetics, isotherm, thermodynamic and mechanism. J Mol Liq 2016;220:432–41.
[96] Sun L, Wan S, Luo W. Biochars prepared from anaerobic digestion residue, palm bark, and eucalyptus for adsorption of cationic methylene blue dye: characterization, equilibrium, and kinetic studies. Bioresour Technol 2013;140:406–13.